Article

Current Biology

Homeostatic Control of Meiotic Prophase Checkpoint Function by Pch2 and Hop1

Graphical Abstract

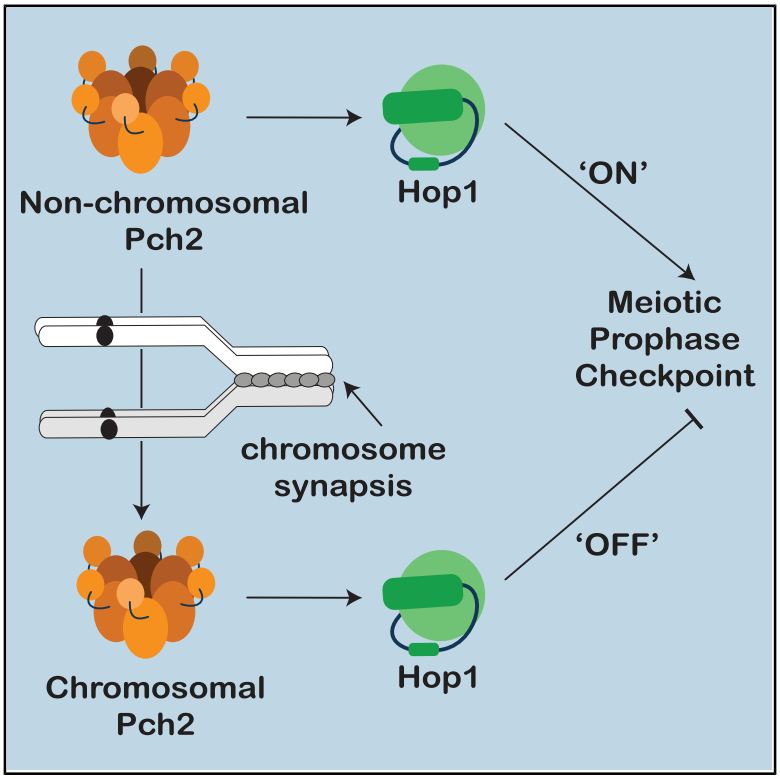

Authors

Vivek B. Raina, Gerben Vader

Correspondence

gerben.vader@mpi-dortmund.mpg.de

In Brief

Raina and Vader demonstrate a general role for budding yeast AAA+ ATPase Pch2, in collaboration with the HORMA protein Hop1, in meiotic prophase checkpoint function. Pch2 can activate or silence checkpoint function. Synaptonemal complex polymerization dictates switch-like behavior of Pch2 function in the meiotic checkpoint.

Highlights

- Feedback regulation between Hop1, Zip1, and Pch2 influences the synaptonemal complex
- Pch2 and Hop1 collaborate to mediate general meiotic prophase checkpoint function
- Pch2 has activating and silencing roles in meiotic prophase checkpoint function
- Synaptonemal complex polymerization dictates switch-like behavior of Pch2 function

Raina & Vader, 2020, Current Biology *30*, 4413–4424
November 16, 2020
https://doi.org/10.1016/j.cub.2020.08.064

CellPress

Current Biology

CellPress
OPEN ACCESS

Article

Homeostatic Control of Meiotic Prophase Checkpoint Function by Pch2 and Hop1

Vivek B. Raina[1,2] and Gerben Vader[1,2,3,*]
[1]Department of Mechanistic Cell Biology, Max Planck Institute of Molecular Physiology, Otto-Hahn-Strasse 11, Dortmund 44227, Germany
[2]International Max Planck Research School (IMPRS) in Chemical and Molecular Biology, Max Planck Institute of Molecular Physiology, Otto-Hahn-Strasse 11, Dortmund 44227, Germany
[3]Lead Contact
*Correspondence: gerben.vader@mpi-dortmund.mpg.de
https://doi.org/10.1016/j.cub.2020.08.064

SUMMARY

Checkpoint cascades link cell cycle progression with essential chromosomal processes. During meiotic prophase, recombination and chromosome synapsis are monitored by what are considered distinct checkpoints. In budding yeast, cells that lack the AAA+ ATPase Pch2 show an impaired cell cycle arrest in response to synapsis defects. However, unperturbed *pch2Δ* cells are delayed in meiotic prophase, suggesting paradoxical roles for Pch2 in cell cycle progression. Here, we provide insight into the checkpoint roles of Pch2 and its connection to Hop1, a HORMA domain-containing client protein. Contrary to current understanding, we find that Pch2 (together with Hop1) is crucial for checkpoint function in response to both recombination and synapsis defects, thus revealing a shared meiotic checkpoint cascade. Meiotic checkpoint responses are transduced by DNA break-dependent phosphorylation of Hop1. Based on our data and on the described effect of Pch2 on HORMA topology, we propose that Pch2 promotes checkpoint proficiency by catalyzing the availability of signaling-competent Hop1. Conversely, we demonstrate that Pch2 can act as a checkpoint silencer, also in the face of persistent DNA repair defects. We establish a framework in which Pch2 and Hop1 form a homeostatic module that governs general meiotic checkpoint function. We show that this module can—depending on the cellular context—fuel or extinguish meiotic checkpoint function, which explains the contradictory roles of Pch2 in cell cycle control. Within the meiotic prophase checkpoint, the Pch2-Hop1 module thus operates analogous to the Pch2/TRIP13-Mad2 module in the spindle assembly checkpoint that monitors chromosome segregation.

INTRODUCTION

During prophase of the meiotic program, controlled double-strand break (DSB) formation and repair takes place, along with synapsis of homologous chromosomes. These processes enable meiotic chromosome segregation and the generation of haploid gametes [1]. Coordination of chromosomal events with cell cycle progression is achieved by checkpoint cascades [2, 3]. In budding yeast, DSB repair is monitored by the recombination checkpoint, which shares similarities with the canonical DNA damage checkpoint, whereas the checkpoint associated with defects in chromosome synapsis is thought to be relayed by distinct signaling machinery [2, 3].

A marker of meiotic prophase progression is the establishment of the synaptonemal complex (SC), which polymerizes between homologous chromosomes, leading to their synapsis. In many organisms, SC polymerization is coupled to crossover recombination [4]. SC polymerization is scaffolded on a meiosis-specific chromosome axis, of which budding yeast Hop1 (or its conserved homologs) forms a key component [5]. Hop1 contains a HORMA domain (for Hop1, Rev7, and Mad2) [6], a structurally conserved domain that can adopt an open/unbuckled or closed conformation [7–9]. (Note that the "open" topology of Hop1 is structurally slightly different from the classical open HORMA topology, and this state is referred to as "unbuckled" [U-]Hop1 [9].) Closed HORMA domains can topologically embrace proteins by engaging with closure motifs (CMs) in interacting proteins [7, 10]. CM-mediated engagement with a binding partner is the active state of HORMA domains, and incorporation of Hop1 into the meiotic chromosome axis is driven by CM-mediated interactions [9, 11–13]. Hop1 binds to a CM in the axis protein Red1 [9]. Hop1 is also a mediator of meiotic prophase checkpoint signaling. It can be phosphorylated by DSB-responsive Mec1/Tel1 kinases [14, 15], leading to the establishment of the Red1-Hop1-Mek1 complex (RHMc), and localized activation of Mek1 kinase, which enforces checkpoint activity [14, 16–18].

A major role for SC establishment is the recruitment of Pch2 (called TRIP13 in mammals), a generally conserved AAA+ ATPase, to chromosomes [19–25]. Pch2 removes Hop1 from the meiotic chromosome axis [7, 23, 26, 27]. As such, Zip1-mediated SC assembly can negatively regulate RHMc-based activity [24, 28, 29]. Pch2 has contrasting effects on cell cycle progression and checkpoint activity. For example, in otherwise unperturbed cells, deletion of Pch2 leads to delayed progression through meiotic prophase [30]. In contrast, in *zip1Δ*, deletion of Pch2 leads to accelerated cell cycle progression, indicative of

a role for Pch2 in synapsis checkpoint function [25, 31]. In *zip1Δ* cells, Pch2 is not associated with chromosomes, except with nucleolar chromatin, but this pool of Pch2 is unlikely to contribute to checkpoint function [25, 32]. The requirement for Pch2 in checkpoint function in *zip1Δ* is seemingly at odds with the described antagonistic role of Pch2 toward Hop1/RHMc-based checkpoint signaling that is associated with Zip1-dependent chromosomal recruitment [7, 23, 26, 27]. Furthermore, *pch2Δ* does not affect cell cycle arrest due to lack of the meiotic RecA homolog crucial for homologous recombination, Dmc1 [30, 33–35]. The distinct behaviors seen for Pch2 under different conditions (i.e., wild type, *zip1Δ*, or *dmc1Δ*) suggest complex Pch2-dependent cell cycle control and independent checkpoint pathways that monitor meiotic prophase.

In multi-cellular eukaryotes, Pch2/TRIP13 also functions in spindle assembly checkpoint (SAC) signaling. Central to SAC signaling is the mitotic checkpoint complex (MCC) [36–39], whose formation depends on a CM-based interaction of closed (C-)Mad2 with Cdc20 [40, 41]. Like Hop1, Mad2 is a HORMA domain protein that can adopt an open (O) or closed state [10, 42]. Crucially, MCC assembly requires sufficient levels of O-Mad2 that are available to be recruited to unattached kinetochores, where the MCC is catalyzed [10, 36, 40–45]. HORMA domains can spontaneously convert from open into closed states, even when not engaged with cognate interaction partners. Pch2/TRIP13 uses its ATPase activity to catalyze the topological conversion of the HORMA domain of Mad2 from the closed to the open form [7, 26, 46, 47]. Without active C-Mad2 to O-Mad2 conversion, driven by Pch2/TRIP13, cells fail to maintain a pool of O-Mad2, impairing MCC catalysis and SAC function [7, 46–53]. Thus, Pch2/TRIP13 contributes to SAC signaling by maintaining sufficient levels of cytoplasmic, signaling-competent O-Mad2 [49, 50]. Because steady-state levels of O-Mad2 are influenced by total Mad2 levels, the total abundance of Mad2 affects the reliance of SAC signaling on Pch2/TRIP13 [48, 50]. The ability of Pch2/TRIP13 to catalyze the transition of C-Mad2 to O-Mad2 is not only required to fuel kinetochore-driven MCC assembly; the same biochemical activity can also lead to disassembly of MCC complexes once proper chromosome-microtubule interactions are established [46, 47, 50, 52, 54, 55]. As such, depending on the cellular context, Pch2/TRIP13 can fuel or silence SAC function.

The functions of Pch2 during progression through meiotic prophase are likely founded on a similar catalytic effect toward the topological state of the HORMA domain of Hop1 [7, 9, 23, 26, 27]. We hypothesize that the seemingly paradoxical roles of Pch2 during meiotic prophase can be explained by signaling logic that shares similarities to that of SAC signaling, where functional consequences of Pch2 action are set by meiosis-specific cellular contexts. Here, we address the basis for the phenotypic behaviors seen in *pch2Δ* cells. We investigate the dynamics of SC assembly and reveal an interplay between Pch2-, Hop1-, and Zip1-dependent SC polymerization. Pch2, in collaboration with Hop1, is required for a shared checkpoint response governing recombination and chromosome synapsis. Depending on the cellular context, Pch2 fulfills checkpoint activating or silencing roles. We build a framework incorporating our findings with established Pch2/HORMA biochemistry to explain the contributions of Pch2 to control of meiotic prophase.

RESULTS

Feedback Regulation between Hop1, Zip1, and Pch2 Influences SC Assembly

To understand the wiring between chromosomal processes during meiotic prophase and the role of Pch2 herein, we investigated the functional relationship between Pch2, the chromosome axis, and SC formation. In this regard, we examined the chromosomal localization of Hop1 and Zip1 (a central SC component) in cells lacking Pch2 during meiotic prophase. We used cells lacking *NDT80*, a transcription factor required for prophase exit [56, 57]. *ndt80Δ* cells arrest after DSB formation has taken place, and crossover repair progresses up to the double Holliday junction stage with fully formed SC [58]. SC polymerization relies on the Hop1-containing chromosome axis [5], and Pch2-dependent removal of Hop1 from chromosomes is enabled upon SC-dependent chromosomal recruitment of Pch2 [19–25]. We detected increased chromosomal association of Hop1 in *pch2Δ* cells (Figures 1A and 1B; *ndt80Δ* and *pch2Δ ndt80Δ* panels) [23, 24]. We note that the total cellular Hop1 in *pch2Δ* cells increase when compared to wild-type cells (Figures S1A and S1B) [24]. We observed a significantly increased chromosomal association of Zip1 in *pch2Δ* as compared with wild-type cells (Figures 1A and 1B; *ndt80Δ* and *pch2Δ ndt80Δ* panels). Thus, Pch2 activity influences the amount of Zip1 that can be deposited on chromosomes. This effect occurred without an obvious effect on total Zip1 levels (Figures S1A and S1B). In total, these findings suggest a role for Pch2 in dynamically modulating Zip1/SC establishment and deposition.

SC factors, such as Zip1, can form extrachromosomal aggregates known as polycomplexes (PCs) [31], which are associated with recombination defects and total levels of Zip1 [28, 59]. The increased association of Zip1 to chromosomes in *pch2Δ* cells prompted us to investigate whether Pch2 influences abundance of PCs. We found that PCs form extensively in *ndt80Δ* cells that display Zip1 SC polymerization (Figures 1A and 1C) [60]. As a note, quantification of PCs was performed only in cells showing extensive polymerization of Zip1 (i.e., "class III" plus PC; Figures 1A, S1C, and S1D). We observed a striking reduction in the frequency of cells displaying Zip1 PCs in cells lacking Pch2 (Figures 1A and 1C, *ndt80Δ* and *pch2Δ ndt80Δ* panels, and S1E and S1F). However, no considerable defects in SC appearance and assembly were observed (either in wild-type or *pch2Δ* cells), regardless of whether these cells had developed PCs (Figure S1G) [25, 31]. The decrease in PCs in *pch2Δ* cells was counterintuitive because DSB repair is delayed under this condition [23, 30, 61, 62]. Hence, if PC formation was a result of DSB defects, an increase in PCs in *pch2Δ* would be expected. These findings suggest that Pch2 influences PC abundance in wild-type conditions. Indeed, loss of Pch2 did not alleviate the accumulation of PCs observed in cells that fail to generate meiotic DSBs (i.e., in *spo11-Y135F* cells; Figures S1H and S1I) [28]. In *ndt80Δ*, the cellular levels of Zip1 continuously rise (Figures S1A and S1B), correlating with the increase in the total number of cells showing PCs (Figure 1C). This suggests that PC formation can be interpreted as a proxy of excess Zip1 remaining after successful establishment of SC.

The reduced prevalence of PCs in *pch2Δ* cells might reflect increased chromosomal levels of Zip1, driven by increased

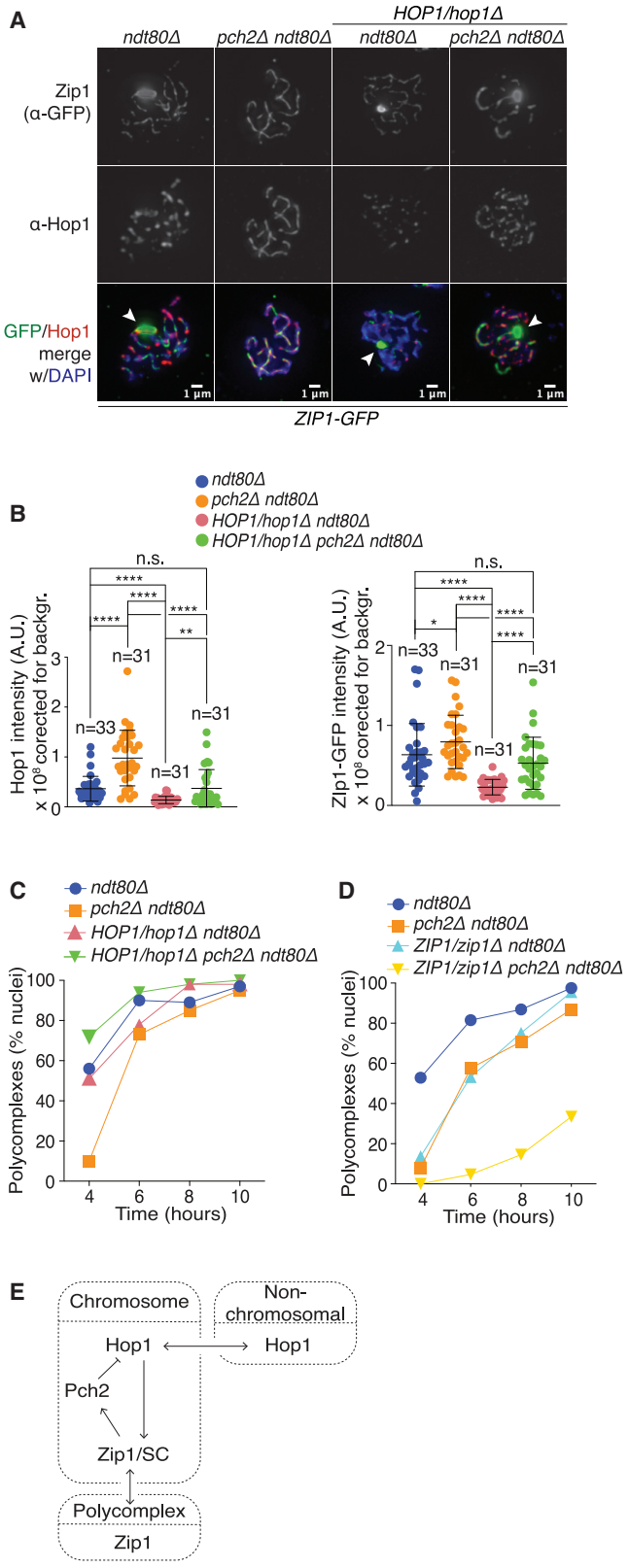

chromosomal Hop1 levels brought about by lack of Pch2-driven removal. We reasoned that reducing the cellular levels of Hop1 would be expected to reduce the fraction of Zip1 on chromosomes and thus trigger increased PC abundance. Following similar logic, reducing Zip1 cellular levels should decrease the presence of excessive Zip1 available for PC formation. Indeed, reducing total levels of Hop1 (by making use of a heterozygous deletion; Figure S2A) led to increased PC abundance in *pch2Δ* cells (Figures 1A and 1C; *HOP1/hop1Δ* panels). Reduction of Hop1 levels resulted in reduced chromosomal levels of Hop1, and Zip1 levels on chromosomes correlated with this behavior (Figures 1A and 1B; *HOP1/hop1Δ* panels), pointing to a relationship between extrachromosomal Zip1 and PC abundance.

In contrast, lowering Zip1 levels (via heterozygous deletion; Figure S2B) reduced PC abundance (Figures 1D and S2C). PC reduction under these conditions was synergistic with *pch2Δ*, potentially reflecting a reduced pool of Zip1 protein available for PC assembly (Figure 1D). These data reveal dynamic Pch2-driven coordination of SC assembly with chromosomally localized Hop1 (Figure 1E).

Pch2 and Hop1 Collaborate to Mediate Prophase Checkpoint Function

Inspired by the functional interplay between Pch2, Hop1 levels, and Zip1/SC assembly, we investigated the roles of Pch2 and Hop1 in cell cycle progression and checkpoint function. *pch2Δ* cells display increased amounts of chromosomal Hop1 (Figures 1A and 1B) [23, 24], and are delayed in meiotic prophase progression [30]. In *zip1Δ*, deletion of Pch2 contrastingly leads to accelerated cell cycle progression [25, 31]. However, *pch2Δ* does not affect cell cycle arrest due to lack of Dmc1 [30, 33–35]. Thus, under different conditions, Pch2 contributes differently to cell cycle control.

To answer the apparent discrepancy of Pch2-associated phenotypes, we investigated whether Hop1 abundance affected cell cycle progression under these three different conditions (i.e., wild type, *zip1Δ*, and *dmc1Δ*). We queried progression through meiotic prophase by analyzing entry into meiosis I/II (scored by spindle morphology) and by activation of Ndt80, which we traced by monitoring expression of Cdc5, a transcriptional target of Ndt80 [57] (Figure 2A). We investigated whether the effects on cell cycle progression were associated with effects on

Figure 1. Feedback Regulation between Hop1, Zip1, and Pch2 Influences SC Assembly

(A) Images of Zip1-GFP (green) and Hop1 (red) immunofluorescence (IF) of chromosome spreads of *ndt80Δ*, *pch2Δndt80Δ*, *HOP1/hop1Δndt80Δ*, and *HOP1/hop1Δpch2Δndt80Δ*. Scale bars indicate 1 μm. Arrowheads indicate polycomplexes.

(B) Quantification of chromosomal intensity of Zip1-GFP and Hop1 on chromosome spreads of strains used in (A). Signal not overlapping with DAPI was excluded, and total sum intensity was background corrected. Mean and standard deviation are indicated. *p ≤ 0.05, **p≤ 0.01, and ****p ≤ 0.0001; Mann-Whitney U test. Number of analyzed cells is indicated. See Data S1.

(C) Percentage of PC-containing cells in *ndt80Δ*, *pch2Δndt80Δ*, *HOP1/hop1Δndt80Δ*, and *HOP1/hop1Δ pch2Δndt80Δ*. >100 nuclei were analyzed.

(D) Cells containing polycomplexes in *ndt80Δ*, *pch2Δndt80Δ*, *ZIP1-GFP/zip1Δndt80Δ*, and *ZIP1-GFP/zip1Δpch2Δndt80Δ*. >100 nuclei were analyzed.

(E) Feedback regulation between Pch2, Zip1, and Hop1. Arrows indicate functional relationships.

See Figures S1 and S2 and Data S1.

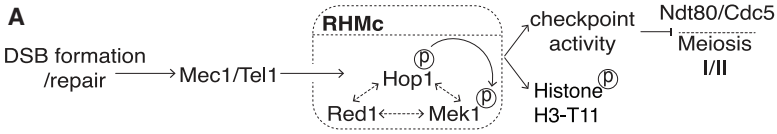

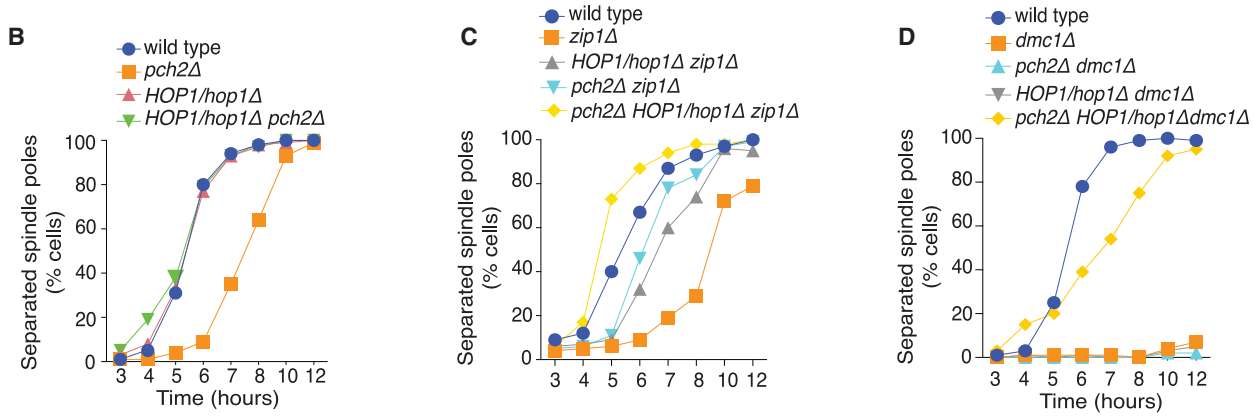

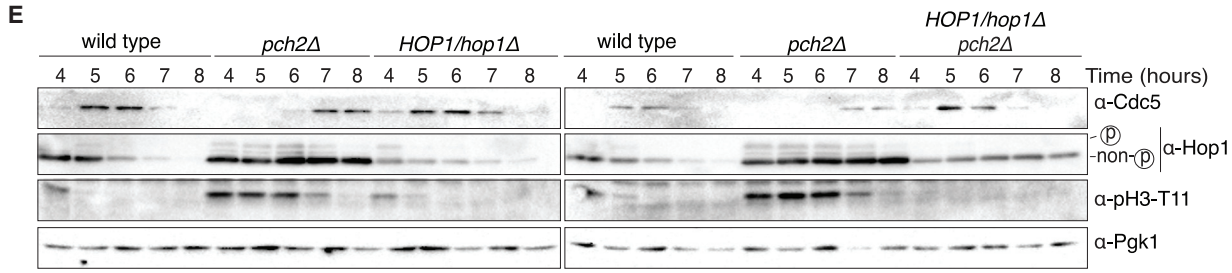

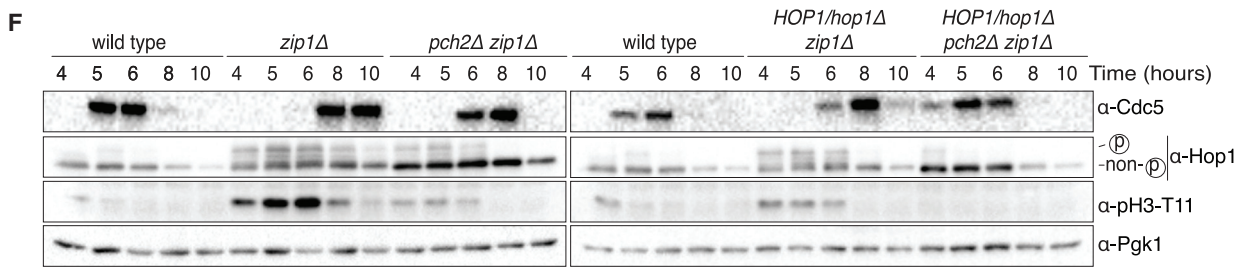

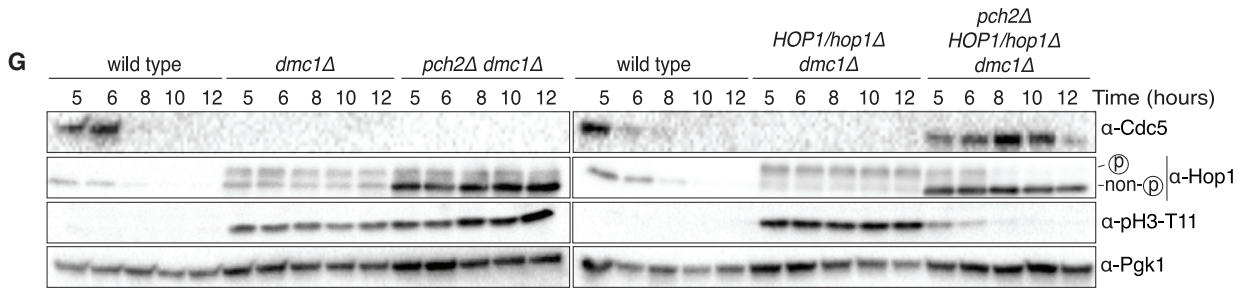

Figure 2. Pch2 and Hop1 Collaborate to Mediate Prophase Checkpoint Function

(A) Cartoon of prophase checkpoint cascade.

(B) Cell cycle progression in wild type, *pch2Δ*, *HOP1/hop1Δ*, and *HOP1/hop1Δ pch2Δ*. >200 cells were counted per data point.

(legend continued on next page)

checkpoint activity by monitoring phospho-status of Hop1 via a well-documented electrophoretic mobility shift (Hop1 is phosphorylated by Mec1/Tel1 kinases in response to checkpoint-activating conditions) [14, 17] and activation of Mek1 by querying the phospho-status of histone H3-threonine 11 (pH3-T11), a Mek1 substrate [63] (Figure 2A). This checkpoint is associated with inhibition of Ndt80 transcriptional activity [64, 65]. Interestingly, reducing Hop1 levels alleviated the prolonged presence of phosphorylated Hop1 and Mek1 activity in *pch2Δ* cells, suggesting untimely activation of Ndt80, as seen by Cdc5 expression (Figure 2E). We observed similar effects between Pch2 and Hop1 when analyzing spore viability (Figure S3A). Therefore, Hop1 protein levels influence Pch2-associated phenotypes beyond SC assembly.

Cells that lack *ZIP1* are delayed in prophase with an active checkpoint [25, 33] (Figures 2C and 2F). As expected, we observed partial alleviation of this checkpoint *zip1Δpch2Δ* cells (Figures 2C and 2F). Intriguingly, *HOP1* heterozygosity alleviated this delay, to an extent that was comparable to that observed in *zip1Δpch2Δ* cells (Figures 2C and 2F). Thus, synapsis checkpoint function requires the correct cellular levels of Hop1. Deleting *PCH2* under conditions of *HOP1* heterozygosity led to even faster progression of the cell cycle (Figure 2C) and reduced phosphorylated Hop1/Mek1 activity as compared to wild-type cells (Figure 2F), indicating that both Pch2 function and Hop1 levels are necessary for optimal checkpoint function. This relation between Pch2 and Hop1 was reflected in spore viability defects (Figure S3B). We investigated the requirements of Pch2 combined with reduced Hop1 levels for checkpoint proficiency in a *zip1Δrad51Δ* background (Rad51 is a RecA-like recombinase). In this background, we observed similar functional checkpoint dysfunction when *pch2Δ* was combined with *HOP1* heterozygosity (Figures S3C and S3D). Our observations indicate an interplay between Pch2 and Hop1 mediating efficient checkpoint response to synapsis defects.

Cells that lack Dmc1 show a near-complete prophase arrest with unrepaired DSBs and Mek1 activation [30, 33] (Figure 2D). *pch2Δ* does not alleviate this arrest [30, 61] (Figure 2D), suggesting that distinct checkpoint responses monitor meiotic prophase, with the contribution of Pch2 limited to synapsis defects [30, 66]. Our observations on the combined effects of *pch2Δ* and reduced Hop1 levels prompted us to revisit the role of Pch2 in recombination checkpoint function. Similar to *pch2Δ*, *HOP1* heterozygosity did not alleviate the *dmc1Δ* arrest (Figures 2D and 2G). However, the combination of *pch2Δ* and *HOP1* heterozygosity led to a robust elimination of checkpoint function in *dmc1Δ* cells (Figures 2D and 2G), indicating that Pch2 acts synergistically with Hop1 in mediating the recombination checkpoint. DSB formation was mildly reduced in *pch2Δ hop1Δ/HOP1* cells (i.e., to ~80% of wild-type levels; Figures S3E and S3F). Similar decreases in DSB levels have been shown to still trigger checkpoint activity [67, 68], ruling out the possibility that checkpoint deficiency in *pch2Δhop1Δ/HOP1* was caused by an indirect effect on meiotic DSB formation. Taken together with our observations on the *zip1Δ* checkpoint response, these data argue that Pch2 and Hop1 are central mediators of both the synapsis and recombination defect-sensing cascades, suggesting the presence of a single checkpoint cascade that monitors meiotic prophase.

SC polymerization is dependent on repair of DSBs, and the recruitment of Pch2 is contingent on SC polymerization [19–25]. The requirement for Pch2 (in combination with reduced Hop1 levels) in mediating checkpoint function observed in both *dmc1Δ* and *zip1Δ* [25] points to a non-chromosomal role for Pch2 in checkpoint activation [32] in *dmc1Δ* and *zip1Δ* cells. Thus, these data suggest that, similar to the contribution of Pch2/TRIP13 to SAC activation (i.e., by maintaining sufficient amounts of O-Mad2 to fuel kinetochore based-SAC signaling) [48–52], Pch2 is needed to maintain the levels of "signaling-competent" Hop1 required for incorporation into "checkpoint-active" chromosomal sites [69].

Pch2 Drives Meiotic Checkpoint Silencing

Catalysis of the transition of C-Mad2 to O-Mad2 by Pch2/TRIP13 is not only required to fuel kinetochore-driven MCC assembly; it can also lead to the disassembly of MCC complexes and SAC silencing [46, 47, 50, 52, 54, 55]. If the role of Pch2 in regulating meiotic checkpoint function is analogous to the function of Pch2/TRIP13 in SAC signaling, it should also exhibit similar checkpoint-antagonizing activities during meiotic prophase. Some observations point in this direction: chromosomally recruited Pch2 can extinguish Mek1-dependent signaling [24], and *pch2Δ* cells are delayed in meiotic prophase with sustained Hop1 phosphorylation (Figures 2B and 2E).

To expose a checkpoint silencing function of Pch2, we wished to identify a condition in which cells fail to establish a checkpoint response despite high levels of DSB-based signaling. Cells that lack both RecA-like DNA recombinases required for DSB repair (i.e., *dmc1Δrad51Δ*) progress past meiotic prophase despite a failure to repair DSBs (Figure 3A) [67, 70]. The reason for this override has remained unclear. We initially investigated the chromosomal recruitment of Gmc2, an SC component [71], in *dmc1Δrad51Δ* cells. Strikingly, we found that *dmc1Δrad51Δ* cells exhibited substantial amounts of chromosomal SC-like structures, whereas *dmc1Δ* cells contained few SC-like chromosomal structures (Figures 3B and 3C). Thus, *dmc1Δrad51Δ* cells form SC structures in a manner that is uncoupled from DSB repair. This suggests that deleting *RAD51* may rescue the *dmc1Δ* arrest by allowing synapsis [72], in turn enabling recruitment of Pch2 to the chromosomes and associated checkpoint silencing. Excitingly, and in line with this idea, removing Pch2 in *dmc1Δrad51Δ* cells prevented entry into meiosis I/II (Figures 3A and 3D, left panel). In accordance with the model that Pch2-dependent checkpoint silencing is executed via extraction

(C) Cell cycle progression in wild type, *zip1Δ*, *HOP1/hop1Δzip1Δ*, *pch2Δzip1Δ*, and *pch2ΔHOP1/hop1Δzip1Δ*. >200 cells were counted per data point.
(D) Cell cycle progression in wild type, *dmc1Δ*, *pch2Δdmc1Δ*, *HOP1/hop1Δ dmc1Δ*, and *pch2ΔHOP1/hop1Δdmc1Δ*. >200 cells were counted per data point.
(E) Western blot analysis of cultures analyzed in (B).
(F) Western blot analysis of cultures analyzed in (C).
(G) Western blot analysis cultures as analyzed in (D).
See Figure S3 and Data S2.

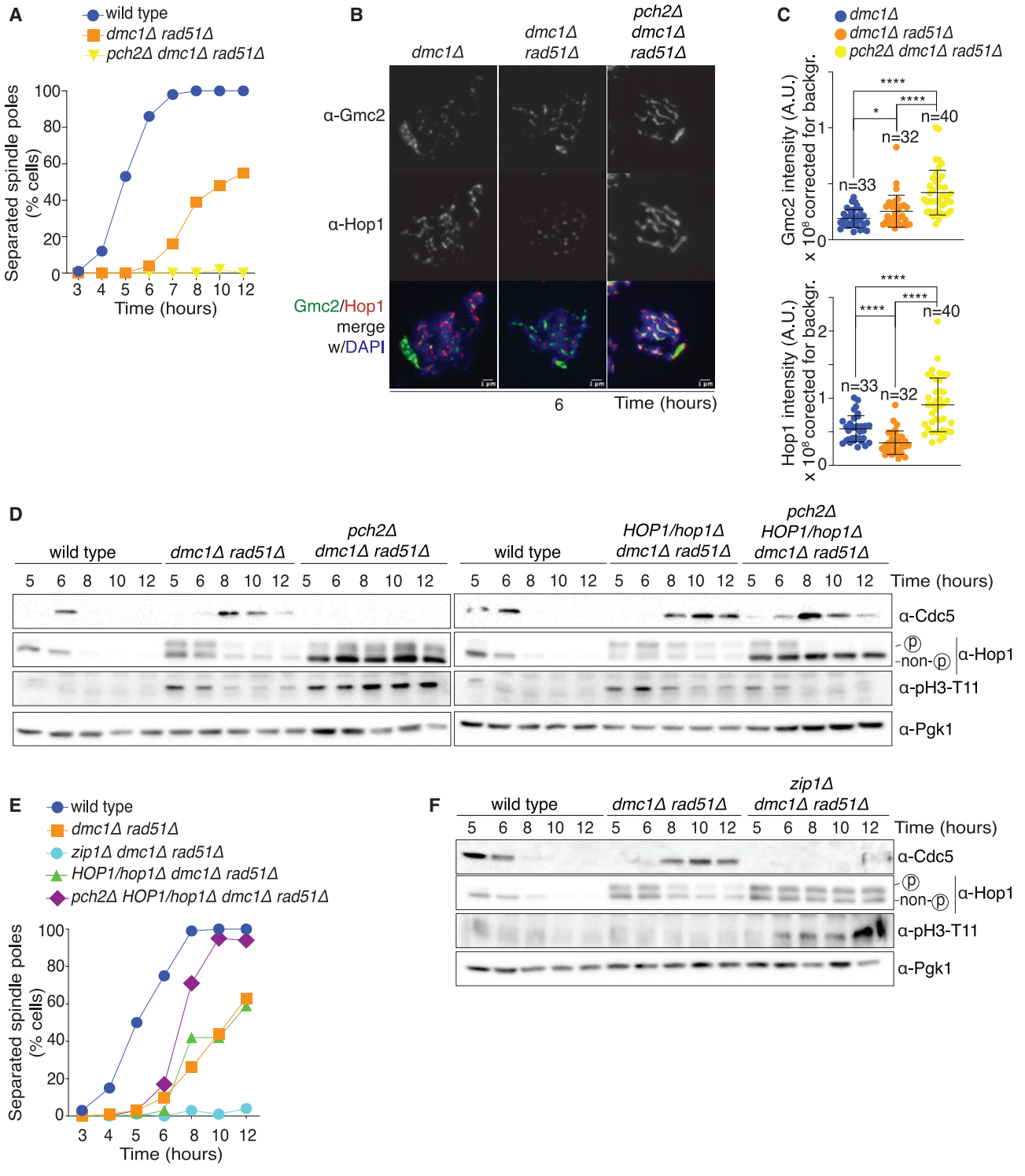

Figure 3. Pch2 Drives Prophase Checkpoint Silencing

(A) Cell cycle progression in wild type, *dmc1Δrad51Δ*, and *pch2Δdmc1Δrad51Δ*. >200 cells were counted for each data point.

(B) Meiotic chromosome spreads from *dmc1Δ*, *dmc1Δrad51Δ*, and *pch2Δ dmc1Δrad51Δ*, stained for Gmc2 (SC component; green) and Hop1 (red). DAPI (blue) is used to stain DNA. Scale bar indicates 1 μm.

(C) Background-corrected chromosomal intensity of Gmc2 and Hop1 as shown in (B). Signal not overlapping with DAPI was excluded. *p ≤ 0.05 and ****p ≤ 0.0001; Mann-Whitney U test. Number of analyzed cells is indicated. See Data S1.

(legend continued on next page)

of Hop1 from chromosomes [24], we found that the amount of Hop1 on chromosomes was significantly higher in *pch2Δdmc1Δrad51Δ* as compared to *dmc1Δrad51Δ* (Figures 3B and 3C). Thus, even in a recombination-deficient condition [67, 70], Pch2 can trigger checkpoint silencing. To show that this checkpoint activity acts via the Pch2-Hop1 cascade, we investigated how Pch2-dependent checkpoint signaling depended on Hop1. The arrest observed in *pch2Δdmc1Δrad51Δ* was alleviated when Hop1 levels were reduced (Figures 3D and 3E), demonstrating that Pch2 and sufficient levels of Hop1 are crucial for establishing checkpoint function, also under these conditions.

Pch2-driven checkpoint silencing in *dmc1Δrad51Δ* cells is predicted to be dependent on SC formation. Indeed, deleting *ZIP1* prevented checkpoint silencing in *dmc1Δrad51Δ* cells (Figures 3E and 3F). These results show that SC-dependent Pch2 function is required for checkpoint silencing, even in the face of unrepaired DSBs. We propose that a key determinant that controls whether Pch2 acts as a checkpoint agonist or antagonist is SC polymerization and thus Pch2 recruitment to chromosomes. Of note, our results suggest that cell cycle progression in *dmc1Δrad51Δ* cells is connected to uncoordinated SC polymerization [67, 70, 72].

Dual Roles of Pch2 in Meiotic Checkpoint Function

To dissect checkpoint silencing and activation functions of Pch2, we established an inducible Pch2-expression system (based on the *pGAL/GAL4-ER* system [73]; Figure 4A). Early expression of Pch2 phenocopied *PCH2* (in terms of Hop1 levels and phosphostatus; Figures S4A and S4B) and did not lead to spore viability defects (Figure S4C), indicating functional expression of Pch2. Expression of Pch2 in *ndt80Δ* cells increased PC abundance, mirroring our earlier observations on the relationship between Pch2, Hop1, and Zip1 (see above; Figures 1 and S4D–S4G). Importantly, induction of Pch2 expression late in meiotic prophase (i.e., at t = 7 h, when extensive Zip1/SC polymerization has taken place; see Figure S1G) led to a rapid reversal of phenotypes associated with sustained checkpoint function in *pch2Δ* cells (i.e., phosphorylated Hop1 and active Mek1; Figure 4B). Thus, under these conditions, Pch2 induction extinguished checkpoint function during meiotic prophase.

We next aimed to create conditions that fail to activate or silence checkpoint function in the absence of Pch2 and investigate the effect of Pch2 induction. With respect to checkpoint activation, we focused on the *zip1Δ* checkpoint response. The expression of Pch2 in a *zip1Δndt80Δ* background led to checkpoint establishment (Figure S4H). Checkpoint activity was already observable, albeit at reduced efficiency, without the induction of Pch2, presumably because of the presence of sufficient levels of Hop1. Indeed, in a *zip1ΔHOP1/hop1Δ* background, we observed a lack of checkpoint signaling without Pch2 induction (Figure 4C). Upon induction of Pch2, robust checkpoint activation was rapidly detected (Figure 4C). Thus, under conditions where Pch2 cannot be recruited to meiotic chromosomes (due to lack of SC formation in *zip1Δ*), expression of Pch2 leads to checkpoint activation, indicating that non-chromosomal Pch2 drives checkpoint activation.

Conversely, induced expression of Pch2 in a *dmc1Δrad51Δ* background led to a rapid decrease of checkpoint-associated markers and entry into meiosis I/II (Figures 4D, 4E, and S5A). This indicates that, upon Pch2 induction, cells rapidly silence checkpoint function in *dmc1Δrad51Δ* cells. Under these conditions, Pch2 can ostensibly be recruited to chromosomes (due to unscheduled SC formation—see above; Figure 3B). Induction of Pch2 in *zip1Δdmc1Δrad51Δ* did not lead to silencing of checkpoint function (Figures S5B and S5C), underscoring the relationship between Zip1-dependent SC formation and Pch2-driven checkpoint inactivation.

Collectively, our data demonstrate that, depending on Zip1-mediated chromosomal context, Pch2 function can lead to opposite outcomes during meiotic prophase: checkpoint activation or inactivation.

DISCUSSION

We provide a framework for checkpoint signaling in meiotic prophase and the homeostatic roles of Pch2 and Hop1 therein (Figures 5A and 5B). We show that Pch2 is important to set a dynamic relationship between chromosomal and non-chromosomal Hop1 and Zip1-dependent synaptonemal complex assembly onto Hop1-containing meiotic chromosomes. We suggest that Zip1-containing PCs are more than merely a consequence of aberrant DSB formation and/or processing [28]: it is a common phenomenon that is related to extent of Zip1-based SC polymerization on chromosomes. This process is quantitatively set by an interplay between Zip1/SC, Hop1, and Pch2 (Figure 1E) and might be influenced by the gradual increase in the level of cellular Zip1 during meiotic prophase (Figures S1A and S1B).

We demonstrate that Pch2 (together with Hop1) is crucial for checkpoint responses to both synapsis and recombination defects. We posit that signaling triggered by these cellular defects share a similar signaling logic: a reliance on the presence/conversion of Hop1 into a topological state (i.e., U-Hop1) that is competent to be rapidly incorporated into chromosome-based checkpoint signaling. Thus, the function of Pch2 in the meiotic prophase checkpoint can be viewed as biochemically analogous to the role of Pch2/TRIP13 in fueling SAC function: by constantly generating the open topological state of a HORMA domain (i.e., Hop1 or Mad2, respectively), Pch2/TRIP13 functions as an engine that provides a substrate (i.e., U-Hop1 or O-Mad2, respectively) available to downstream signaling machineries that generate the biochemical entities enforcing cell cycle arrest (i.e., chromosome-based, Mec1/Tel-activated RHMc or kinetochore-based MCC, respectively). In line with the idea that the responses to recombination and synapsis defects are relayed by a shared cascade is the observation that the synapsis checkpoint relies on meiotic DSB formation [74].

(D) Western blot analysis in wild type, *dmc1Δrad51Δ*, *pch2Δdmc1Δrad51Δ*, *HOP1/hop1Δdmc1Δrad51Δ*, and *pch2ΔHOP1/hop1Δdmc1Δrad51Δ*. Samples are from the same experiment as shown in (E).
(E) Cell cycle progression in strains described in (D), with the addition of *zip1Δ dmc1Δ rad51Δ*. >200 cells were counted for each data point.
(F) Western blot analysis in wild type, *dmc1Δ rad51Δ*, and *zip1Δ dmc1Δ rad51Δ*.

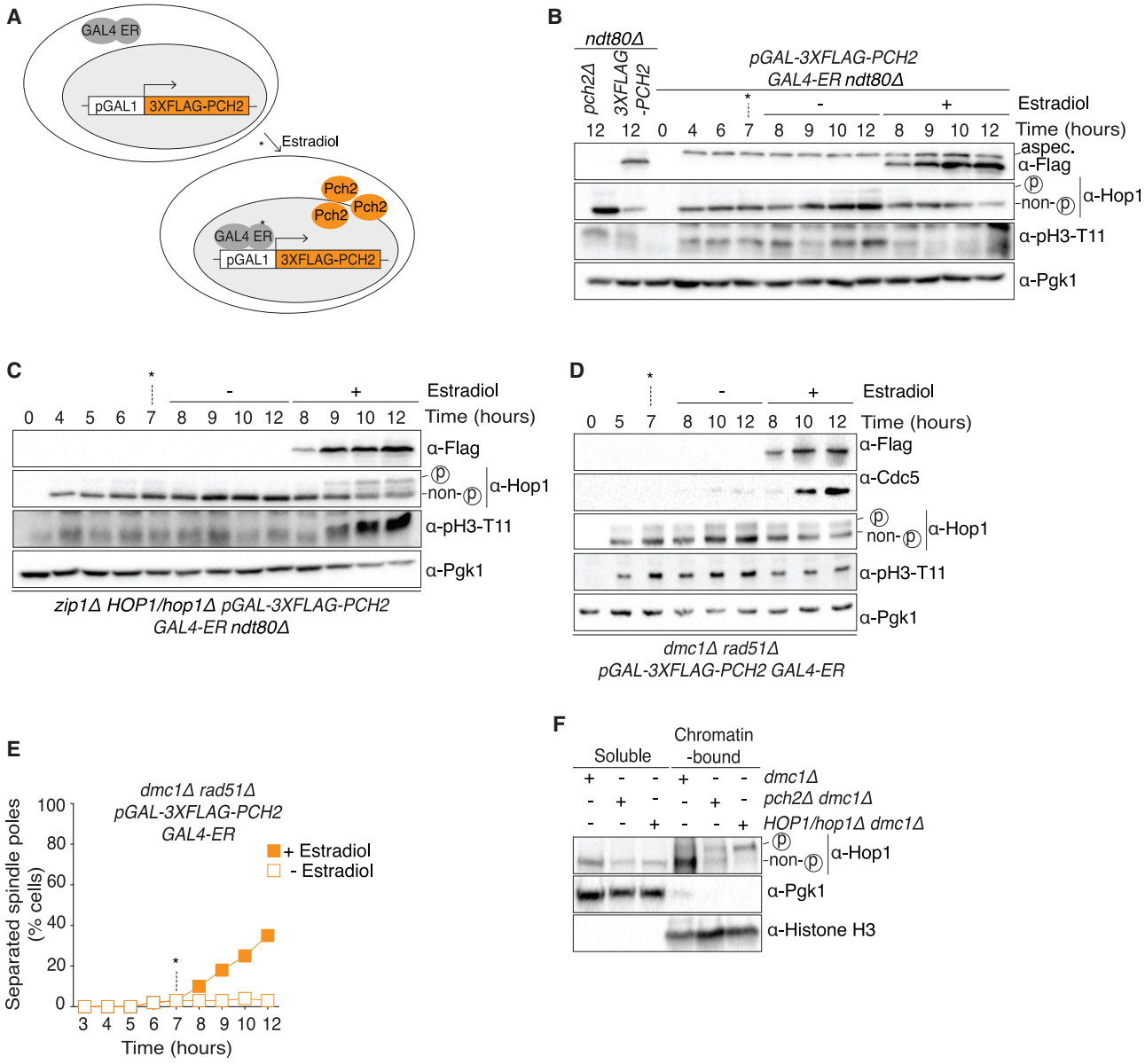

Figure 4. Dual Roles of the Pch2/Hop1

(A) Schematic showing the *pGAL1-3XFLAG-PCH2 GAL4-ER* system.

(B) Western blot analysis with and without induction of Pch2 in *ndt80Δ*, compared to *pch2Δndt80Δ* and *pPCH2-3XFLAG-PCH2ndt80Δ*. * indicates estradiol addition.

(C) Western blot analysis with and without induction of Pch2 in *zip1ΔHOP1/hop1Δndt80Δ*. * indicates estradiol addition.

(D) Western blot analysis with and without induction of Pch2 in *dmc1Δrad51Δ*. * indicates estradiol addition.

(E) Cell cycle progression with and without induction of Pch2 in *dmc1Δrad51Δ*. Estradiol was added 7 h post-induction of meiosis (indicated by *).

(F) Chromatin fractionations for *dmc1Δ*, *pch2Δdmc1Δ*, *HOP1/hop1Δdmc1Δ* (7 h post-induction of meiosis). Histone H3 and Pgk1 are chromatin and soluble fraction markers, respectively.

See Figures S4 and S5 and Data S2.

This model should be extended to explain why, under certain conditions, Pch2 is redundant in mounting a checkpoint response (e.g., in *dmc1Δ*, if Hop1 levels are not interfered with). We postulate that a sufficient concentration of the signaling-competent form of Hop1 (dictated by the equilibrium between the two states of Hop1 and Hop1 total protein levels), proficient to be incorporated in RHMc, exists, even without Pch2. Evidently, in the absence of Pch2, such a system can only generate productive signaling once high levels of Mec1/Tel1-based signaling is present (as is the case in *dmc1Δ* cells) [14, 30, 33] and when normal levels of Hop1 are maintained (as shown here). This predicts that sufficient levels of signaling-competent Hop1 are maintained in *dmc1Δ* when either Pch2 or Hop1 levels are interfered with. This was indeed the case: in

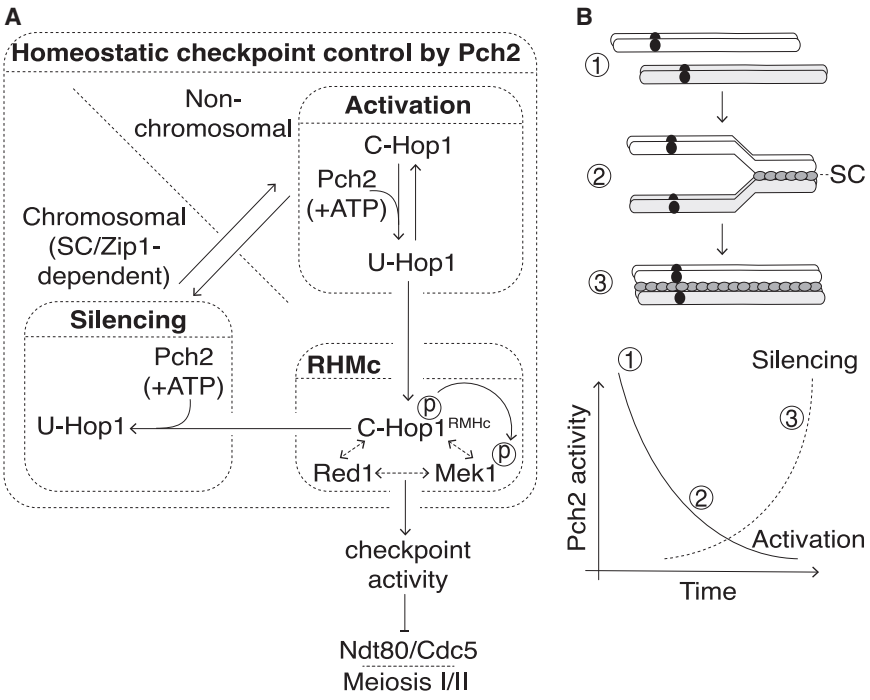

Figure 5. Model of Pch2 in Meiotic Checkpoint Function

(A and B) Schematics highlighting the dual role of Pch2 in prophase checkpoint function, related to ongoing chromosome synapsis, as indicated by SC formation between homologous chromosomes.

Non-chromosomal Pch2 aids checkpoint activity by promoting the availability of U-Hop1, whereas chromosomal Pch2 promotes checkpoint complex disassembly and checkpoint silencing by converting C-Hop1 that is present in an active signaling complex (i.e., RHMc). SC polymerization, which drives chromosomal association of Pch2, provides a switch in "client" preference during meiotic prophase (Figure 5B). In the analogy with SAC regulation and MCC disassembly, SC formation can conceptually be equated with chromosome bi-orientation during mitosis: the cytological state when MCC disassembly needs to be promoted [46, 47, 55]. Pch2 is likely not the only factor that contributes to meiotic checkpoint silencing (*pch2Δ* cells eventually exit meiotic prophase; e.g., Figures 2B and 2E), arguing for additional checkpoint inactivation pathways [75], as is the case for SAC/MCC inactivation [49, 76].

dmc1Δ, pch2Δ dmc1Δ, HOP1/hop1Δ dmc1Δ cells, the phosphorylated form of Hop1 was maintained, whereas in *pch2Δ HOP1/hop1Δ dmc1Δ*, this form of Hop1 was rapidly lost (Figure 2G). Furthermore, the phosphorylated pool of Hop1 (which was specifically enriched within chromatin-associated Hop1, in line with the idea of chromosome-based checkpoint catalysis) was maintained at similar levels in *dmc1Δ, pch2Δdmc1Δ* or *HOP1/hop1Δdmc1Δ* cells (Figure 4F).

Under less extreme kinase signaling conditions (e.g., in wild-type or *zip1Δ* cells), or when Hop1 levels are compromised, Pch2 becomes crucial to generate a large enough pool of checkpoint-competent Hop1 that can be incorporated into chromosome-based signaling. In *pch2Δ*, total cellular Hop1 levels are increased (e.g., Figures S1A and S1B). This increase might reflect in higher absolute concentration of U-Hop1 present within the cell, thus bypassing the role of Pch2 in RHMc-based checkpoint signaling. Although U- and C-Hop1 have been described to exist *in vitro* [9], it will be important in the future to confirm the presence of these Hop1 conformers *in vivo* and investigate their dynamics in relation to Pch2 activity. The dependence of checkpoint function on Pch2 activity is influenced by the protein levels of its client Hop1, which is reminiscent of the influence Mad2 levels has on Pch2/TRIP13-dependent SAC response in multi-cellular eukaryotes [48, 50]. Similar observations have been made using overexpression of Hop1 with respect to Pch2-mediated checkpoint function [69]. In light of our findings, it will be interesting to test the requirement of Pch2/TRIP13 (and Mad2 levels) in SAC signaling under conditions that trigger subtle checkpoint-activating conditions (comparable to *zip1Δ* in the case of meiotic prophase).

Pch2 can also lead to checkpoint silencing. We propose that both checkpoint activation and inactivation functions of Pch2 are derived from the same biochemical reaction: topological conversion of Hop1. Depending on the subcellular localization and context, this catalysis can lead to distinctly different outcomes.

We also note a fascinating distinction between these cell cycle checkpoints: meiotic HORMA proteins (i.e., Hop1 and homologs) are unique in that they encode a closure motif in their COOH terminus [7–9]. Without active conversion, intramolecular closed HORMA-CM interactions (that are predicted to generate "inactivated" C-Hop1 proteins; intra-C-Hop1) seem inevitable. This implies that once Pch2 recruitment to chromosomes upon SC formation is complete, Pch2-dependent release of Hop1 from chromosomes should rapidly lead to a large pool of inactive, non-chromosomal intra-C-Hop1. We speculate that this characteristic might instate "switch-like" behavior in checkpoint function downstream of SC-dependent recruitment of Pch2, as also recently suggested by the interplay between PCH2 and ASY1, the Hop1 homolog in *Arabidopsis thaliana* [77].

Revealing the biochemical basis of Pch2 recruitment to chromosomes and understanding whether additional regulation drives the switch of Pch2 from monomeric, non-chromosomal C-Hop1 to chromosome-associated C-Hop1 are questions that warrant investigation. Finally, the fact that two checkpoint cascades—the prophase checkpoint and spindle assembly checkpoint—that respond to distinct chromosomal defects show analogous signaling logic raises fascinating questions regarding the evolutionary origin of these essential signaling pathways [78].

STAR★METHODS

Detailed methods are provided in the online version of this paper and include the following:

SUPPLEMENTAL INFORMATION

Supplemental Information can be found online at https://doi.org/10.1016/j.cub.2020.08.064.

ACKNOWLEDGMENTS

We thank the Vader and Bird laboratories for ideas and discussions. We thank Divya Singh for helpful discussions on the experimental design. We thank Andrea Musacchio for ongoing support throughout this project. We thank Adèle Marston, John Weir, Andrea Musacchio, Marcel van Vugt, Divya Singh, Vaishnavi Nivsarkar, Richard Cardoso da Silva, and Arnaud Rondelet for comments on the manuscript. We acknowledge Amy MacQueen for sharing reagents. This work was financially supported by the European Research Council (ERC starting grant URDNA, agreement no. 638197, to G.V.) and the Max Planck Society. The ORCIDs for this article are 0000-0003-0507-9208 (V.B.R.) and 0000-0001-5729-0991 (G.V.).

AUTHOR CONTRIBUTIONS

V.B.R. conceptualized the idea and model of this study and performed experiments and analysis, with the exception of Southern blot analysis, which was performed by G.V. V.B.R. and G.V. conceived and designed experiments and wrote the manuscript. G.V. supervised the study and acquired funds.

DECLARATION OF INTERESTS

The authors declare no competing interests.

Received: April 24, 2020
Revised: July 31, 2020
Accepted: August 18, 2020
Published: September 10, 2020

REFERENCES

1. Petronczki, M., Siomos, M.F., and Nasmyth, K. (2003). Un ménage à quatre: the molecular biology of chromosome segregation in meiosis. Cell *112*, 423–440.
2. Subramanian, V.V., and Hochwagen, A. (2014). The meiotic checkpoint network: step-by-step through meiotic prophase. Cold Spring Harb. Perspect. Biol. *6*, a016675.
3. Hochwagen, A., and Amon, A. (2006). Checking your breaks: surveillance mechanisms of meiotic recombination. Curr. Biol. *16*, R217–R228.
4. Hunter, N. (2015). Meiotic recombination: the essence of heredity. Cold Spring Harb. Perspect. Biol. *7*, a016618.
5. Hollingsworth, N.M., and Byers, B. (1989). HOP1: a yeast meiotic pairing gene. Genetics *121*, 445–462.
6. Aravind, L., and Koonin, E.V. (1998). The HORMA domain: a common structural denominator in mitotic checkpoints, chromosome synapsis and DNA repair. Trends Biochem. Sci. *23*, 284–286.
7. Rosenberg, S.C., and Corbett, K.D. (2015). The multifaceted roles of the HORMA domain in cellular signaling. J. Cell Biol. *211*, 745–755.
8. Kim, Y., Rosenberg, S.C., Kugel, C.L., Kostow, N., Rog, O., Davydov, V., Su, T.Y., Dernburg, A.F., and Corbett, K.D. (2014). The chromosome axis controls meiotic events through a hierarchical assembly of HORMA domain proteins. Dev. Cell *31*, 487–502.
9. West, A.M.V., Komives, E.A., and Corbett, K.D. (2018). Conformational dynamics of the Hop1 HORMA domain reveal a common mechanism with the spindle checkpoint protein Mad2. Nucleic Acids Res. *46*, 279–292.
10. Mapelli, M., and Musacchio, A. (2007). MAD contortions: conformational dimerization boosts spindle checkpoint signaling. Curr. Opin. Struct. Biol. *17*, 716–725.
11. West, A.M., Rosenberg, S.C., Ur, S.N., Lehmer, M.K., Ye, Q., Hagemann, G., Caballero, I., Usón, I., MacQueen, A.J., Herzog, F., and Corbett, K.D. (2019). A conserved filamentous assembly underlies the structure of the meiotic chromosome axis. eLife *8*, e40372.
12. Hollingsworth, N.M., and Ponte, L. (1997). Genetic interactions between *HOP1, RED1* and *MEK1* suggest that *MEK1* regulates assembly of axial element components during meiosis in the yeast Saccharomyces cerevisiae. Genetics *147*, 33–42.
13. Woltering, D., Baumgartner, B., Bagchi, S., Larkin, B., Loidl, J., de los Santos, T., and Hollingsworth, N.M. (2000). Meiotic segregation, synapsis, and recombination checkpoint functions require physical interaction between the chromosomal proteins Red1p and Hop1p. Mol. Cell. Biol. *20*, 6646–6658.
14. Carballo, J.A., Johnson, A.L., Sedgwick, S.G., and Cha, R.S. (2008). Phosphorylation of the axial element protein Hop1 by Mec1/Tel1 ensures meiotic interhomolog recombination. Cell *132*, 758–770.
15. de los Santos, T., and Hollingsworth, N.M. (1999). Red1p, a *MEK1*-dependent phosphoprotein that physically interacts with Hop1p during meiosis in yeast. J. Biol. Chem. *274*, 1783–1790.
16. Bailis, J.M., and Roeder, G.S. (1998). Synaptonemal complex morphogenesis and sister-chromatid cohesion require Mek1-dependent phosphorylation of a meiotic chromosomal protein. Genes Dev. *12*, 3551–3563.
17. Niu, H., Wan, L., Baumgartner, B., Schaefer, D., Loidl, J., and Hollingsworth, N.M. (2005). Partner choice during meiosis is regulated by Hop1-promoted dimerization of Mek1. Mol. Biol. Cell *16*, 5804–5818.
18. Niu, H., Li, X., Job, E., Park, C., Moazed, D., Gygi, S.P., and Hollingsworth, N.M. (2007). Mek1 kinase is regulated to suppress double-strand break repair between sister chromatids during budding yeast meiosis. Mol. Cell. Biol. *27*, 5456–5467.
19. Wojtasz, L., Daniel, K., Roig, I., Bolcun-Filas, E., Xu, H., Boonsanay, V., Eckmann, C.R., Cooke, H.J., Jasin, M., Keeney, S., et al. (2009). Mouse HORMAD1 and HORMAD2, two conserved meiotic chromosomal proteins, are depleted from synapsed chromosome axes with the help of TRIP13 AAA-ATPase. PLoS Genet. *5*, e1000702.
20. Roig, I., Dowdle, J.A., Toth, A., de Rooij, D.G., Jasin, M., and Keeney, S. (2010). Mouse TRIP13/PCH2 is required for recombination and normal higher-order chromosome structure during meiosis. PLoS Genet. *6*, e1001062.

21. Li, X.C., and Schimenti, J.C. (2007). Mouse pachytene checkpoint 2 (trip13) is required for completing meiotic recombination but not synapsis. PLoS Genet. *3*, e130.

22. Joshi, N., Barot, A., Jamison, C., and Börner, G.V. (2009). Pch2 links chromosome axis remodeling at future crossover sites and crossover distribution during yeast meiosis. PLoS Genet. *5*, e1000557.

23. Börner, G.V., Barot, A., and Kleckner, N. (2008). Yeast Pch2 promotes domainal axis organization, timely recombination progression, and arrest of defective recombinosomes during meiosis. Proc. Natl. Acad. Sci. USA *105*, 3327–3332.

24. Subramanian, V.V., MacQueen, A.J., Vader, G., Shinohara, M., Sanchez, A., Borde, V., Shinohara, A., and Hochwagen, A. (2016). Chromosome synapsis alleviates Mek1-dependent suppression of meiotic DNA repair. PLoS Biol. *14*, e1002369.

25. San-Segundo, P.A., and Roeder, G.S. (1999). Pch2 links chromatin silencing to meiotic checkpoint control. Cell *97*, 313–324.

26. Vader, G. (2015). Pch2(TRIP13): controlling cell division through regulation of HORMA domains. Chromosoma *124*, 333–339.

27. Chen, C., Jomaa, A., Ortega, J., and Alani, E.E. (2014). Pch2 is a hexameric ring ATPase that remodels the chromosome axis protein Hop1. Proc. Natl. Acad. Sci. USA *111*, E44–E53.

28. Henderson, K.A., and Keeney, S. (2004). Tying synaptonemal complex initiation to the formation and programmed repair of DNA double-strand breaks. Proc. Natl. Acad. Sci. USA *101*, 4519–4524.

29. Börner, G.V., Kleckner, N., and Hunter, N. (2004). Crossover/noncrossover differentiation, synaptonemal complex formation, and regulatory surveillance at the leptotene/zygotene transition of meiosis. Cell *117*, 29–45.

30. Hochwagen, A., Tham, W.H., Brar, G.A., and Amon, A. (2005). The FK506 binding protein Fpr3 counteracts protein phosphatase 1 to maintain meiotic recombination checkpoint activity. Cell *122*, 861–873.

31. Sym, M., Engebrecht, J.A., and Roeder, G.S. (1993). *ZIP1* is a synaptonemal complex protein required for meiotic chromosome synapsis. Cell *72*, 365–378.

32. Herruzo, E., Santos, B., Freire, R., Carballo, J.A., and San-Segundo, P.A. (2019). Characterization of Pch2 localization determinants reveals a nucleolar-independent role in the meiotic recombination checkpoint. Chromosoma *128*, 297–316.

33. Xu, L., Weiner, B.M., and Kleckner, N. (1997). Meiotic cells monitor the status of the interhomolog recombination complex. Genes Dev. *11*, 106–118.

34. Bishop, D.K., Park, D., Xu, L., and Kleckner, N. (1992). *DMC1*: a meiosis-specific yeast homolog of E. coli recA required for recombination, synaptonemal complex formation, and cell cycle progression. Cell *69*, 439–456.

35. Schwacha, A., and Kleckner, N. (1997). Interhomolog bias during meiotic recombination: meiotic functions promote a highly differentiated interhomolog-only pathway. Cell *90*, 1123–1135.

36. Faesen, A.C., Thanasoula, M., Maffini, S., Breit, C., Müller, F., van Gerwen, S., Bange, T., and Musacchio, A. (2017). Basis of catalytic assembly of the mitotic checkpoint complex. Nature *542*, 498–502.

37. Fraschini, R., Beretta, A., Lucchini, G., and Piatti, S. (2001). Role of the kinetochore protein Ndc10 in mitotic checkpoint activation in Saccharomyces cerevisiae. Mol. Genet. Genomics *266*, 115–125.

38. Sudakin, V., Chan, G.K., and Yen, T.J. (2001). Checkpoint inhibition of the APC/C in HeLa cells is mediated by a complex of BUBR1, BUB3, CDC20, and MAD2. J. Cell Biol. *154*, 925–936.

39. Hardwick, K.G., Johnston, R.C., Smith, D.L., and Murray, A.W. (2000). MAD3 encodes a novel component of the spindle checkpoint which interacts with Bub3p, Cdc20p, and Mad2p. J. Cell Biol. *148*, 871–882.

40. Sironi, L., Mapelli, M., Knapp, S., De Antoni, A., Jeang, K.T., and Musacchio, A. (2002). Crystal structure of the tetrameric Mad1-Mad2 core complex: implications of a 'safety belt' binding mechanism for the spindle checkpoint. EMBO J. *21*, 2496–2506.

41. Luo, X., Tang, Z., Rizo, J., and Yu, H. (2002). The Mad2 spindle checkpoint protein undergoes similar major conformational changes upon binding to either Mad1 or Cdc20. Mol. Cell *9*, 59–71.

42. Mapelli, M., Massimiliano, L., Santaguida, S., and Musacchio, A. (2007). The Mad2 conformational dimer: structure and implications for the spindle assembly checkpoint. Cell *131*, 730–743.

43. Rieder, C.L., Cole, R.W., Khodjakov, A., and Sluder, G. (1995). The checkpoint delaying anaphase in response to chromosome monoorientation is mediated by an inhibitory signal produced by unattached kinetochores. J. Cell Biol. *130*, 941–948.

44. Simonetta, M., Manzoni, R., Mosca, R., Mapelli, M., Massimiliano, L., Vink, M., Novak, B., Musacchio, A., and Ciliberto, A. (2009). The influence of catalysis on mad2 activation dynamics. PLoS Biol. *7*, e10.

45. Kulukian, A., Han, J.S., and Cleveland, D.W. (2009). Unattached kinetochores catalyze production of an anaphase inhibitor that requires a Mad2 template to prime Cdc20 for BubR1 binding. Dev. Cell *16*, 105–117.

46. Ye, Q., Kim, D.H., Dereli, I., Rosenberg, S.C., Hagemann, G., Herzog, F., Tóth, A., Cleveland, D.W., and Corbett, K.D. (2017). The AAA+ ATPase TRIP13 remodels HORMA domains through N-terminal engagement and unfolding. EMBO J. *36*, 2419–2434.

47. Alfieri, C., Chang, L., and Barford, D. (2018). Mechanism for remodelling of the cell cycle checkpoint protein MAD2 by the ATPase TRIP13. Nature *559*, 274–278.

48. Marks, D.H., Thomas, R., Chin, Y., Shah, R., Khoo, C., and Benezra, R. (2017). Mad2 overexpression uncovers a critical role for TRIP13 in mitotic exit. Cell Rep. *19*, 1832–1845.

49. Ma, H.T., and Poon, R.Y.C. (2018). TRIP13 functions in the establishment of the spindle assembly checkpoint by replenishing O-MAD2. Cell Rep. *22*, 1439–1450.

50. Kim, D.H., Han, J.S., Ly, P., Ye, Q., McMahon, M.A., Myung, K., Corbett, K.D., and Cleveland, D.W. (2018). TRIP13 and APC15 drive mitotic exit by turnover of interphase- and unattached kinetochore-produced MCC. Nat. Commun. *9*, 4354.

51. Nelson, C.R., Hwang, T., Chen, P.H., and Bhalla, N. (2015). *TRIP13PCH-2* promotes Mad2 localization to unattached kinetochores in the spindle checkpoint response. J. Cell Biol. *211*, 503–516.

52. Ma, H.T., and Poon, R.Y.C. (2016). *TRIP13* regulates both the activation and inactivation of the spindle-assembly checkpoint. Cell Rep. *14*, 1086–1099.

53. Yost, S., de Wolf, B., Hanks, S., Zachariou, A., Marcozzi, C., Clarke, M., de Voer, R., Etemad, B., Uijttewaal, E., Ramsay, E., et al. (2017). Biallelic *TRIP13* mutations predispose to Wilms tumor and chromosome missegregation. Nat. Genet. *49*, 1148–1151.

54. Wang, K., Sturt-Gillespie, B., Hittle, J.C., Macdonald, D., Chan, G.K., Yen, T.J., and Liu, S.T. (2014). Thyroid hormone receptor interacting protein 13 (TRIP13) AAA-ATPase is a novel mitotic checkpoint-silencing protein. J. Biol. Chem. *289*, 23928–23937.

55. Eytan, E., Wang, K., Miniowitz-Shemtov, S., Sitry-Shevah, D., Kaisari, S., Yen, T.J., Liu, S.T., and Hershko, A. (2014). Disassembly of mitotic checkpoint complexes by the joint action of the AAA-ATPase TRIP13 and p31(comet). Proc. Natl. Acad. Sci. USA *111*, 12019–12024.

56. Xu, L., Ajimura, M., Padmore, R., Klein, C., and Kleckner, N. (1995). *NDT80*, a meiosis-specific gene required for exit from pachytene in Saccharomyces cerevisiae. Mol. Cell. Biol. *15*, 6572–6581.

57. Sourirajan, A., and Lichten, M. (2008). Polo-like kinase Cdc5 drives exit from pachytene during budding yeast meiosis. Genes Dev. *22*, 2627–2632.

58. Allers, T., and Lichten, M. (2001). Differential timing and control of noncrossover and crossover recombination during meiosis. Cell *106*, 47–57.

59. Sym, M., and Roeder, G.S. (1995). Zip1-induced changes in synaptonemal complex structure and polycomplex assembly. J. Cell Biol. *128*, 455–466.

60. Bhuiyan, H., Dahlfors, G., and Schmekel, K. (2003). Lateral elements inside synaptonemal complex-like polycomplexes in *ndt80* mutants of yeast bind DNA. Genetics *163*, 539–544.

61. Wu, H.Y., and Burgess, S.M. (2006). Two distinct surveillance mechanisms monitor meiotic chromosome metabolism in budding yeast. Curr. Biol. *16*, 2473–2479.

62. Joshi, N., Brown, M.S., Bishop, D.K., and Börner, G.V. (2015). Gradual implementation of the meiotic recombination program via checkpoint pathways controlled by global DSB levels. Mol. Cell *57*, 797–811.

63. Kniewel, R., Murakami, H., Liu, Y., Ito, M., Ohta, K., Hollingsworth, N.M., and Keeney, S. (2017). Histone H3 threonine 11 phosphorylation is catalyzed directly by the meiosis-specific kinase Mek1 and provides a molecular readout of Mek1 activity *in vivo*. Genetics *207*, 1313–1333.

64. Hollingsworth, N.M., and Gaglione, R. (2019). The meiotic-specific Mek1 kinase in budding yeast regulates interhomolog recombination and coordinates meiotic progression with double-strand break repair. Curr. Genet. *65*, 631–641.

65. Chen, X., Gaglione, R., Leong, T., Bednor, L., de Los Santos, T., Luk, E., Airola, M., and Hollingsworth, N.M. (2018). Mek1 coordinates meiotic progression with DNA break repair by directly phosphorylating and inhibiting the yeast pachytene exit regulator Ndt80. PLoS Genet. *14*, e1007832.

66. Ho, H.C., and Burgess, S.M. (2011). Pch2 acts through Xrs2 and Tel1/ATM to modulate interhomolog bias and checkpoint function during meiosis. PLoS Genet. *7*, e1002351.

67. Markowitz, T.E., Suarez, D., Blitzblau, H.G., Patel, N.J., Markhard, A.L., MacQueen, A.J., and Hochwagen, A. (2017). Reduced dosage of the chromosome axis factor Red1 selectively disrupts the meiotic recombination checkpoint in *Saccharomyces cerevisiae*. PLoS Genet. *13*, e1006928.

68. Zanders, S., and Alani, E. (2009). The *pch2Delta* mutation in baker's yeast alters meiotic crossover levels and confers a defect in crossover interference. PLoS Genet. *5*, e1000571.

69. Herruzo, E., Ontoso, D., González-Arranz, S., Cavero, S., Lechuga, A., and San-Segundo, P.A. (2016). The Pch2 AAA+ ATPase promotes phosphorylation of the Hop1 meiotic checkpoint adaptor in response to synaptonemal complex defects. Nucleic Acids Res. *44*, 7722–7741.

70. Shinohara, A., Gasior, S., Ogawa, T., Kleckner, N., and Bishop, D.K. (1997). Saccharomyces cerevisiae recA homologues *RAD51* and *DMC1* have both distinct and overlapping roles in meiotic recombination. Genes Cells *2*, 615–629.

71. Humphryes, N., Leung, W.K., Argunhan, B., Terentyev, Y., Dvorackova, M., and Tsubouchi, H. (2013). The Ecm11-Gmc2 complex promotes synaptonemal complex formation through assembly of transverse filaments in budding yeast. PLoS Genet. *9*, e1003194.

72. Zhang, F., Shen, Y., Miao, C., Cao, Y., Shi, W., Du, G., Tang, D., Li, Y., Luo, Q., and Cheng, Z. (2020). *OsRAD51D* promotes homologous pairing and recombination by preventing nonhomologous interactions in rice meiosis. New Phytol. *227*, 824–839.

73. Benjamin, K.R., Zhang, C., Shokat, K.M., and Herskowitz, I. (2003). Control of landmark events in meiosis by the CDK Cdc28 and the meiosis-specific kinase Ime2. Genes Dev. *17*, 1524–1539.

74. González-Arranz, S., Cavero, S., Morillo-Huesca, M., Andújar, E., Pérez-Alegre, M., Prado, F., and San-Segundo, P. (2018). Functional impact of the H2A.Z histone variant during meiosis in *Saccharomyces cerevisiae*. Genetics *209*, 997–1015.

75. Bailis, J.M., and Roeder, G.S. (2000). Pachytene exit controlled by reversal of Mek1-dependent phosphorylation. Cell *101*, 211–221.

76. Kaisari, S., Sitry-Shevah, D., Miniowitz-Shemtov, S., Teichner, A., and Hershko, A. (2017). Role of CCT chaperonin in the disassembly of mitotic checkpoint complexes. Proc. Natl. Acad. Sci. USA *114*, 956–961.

77. Yang, C., Hu, B., Portheine, S.M., Chuenban, P., and Schnittger, A. (2020). State changes of the HORMA protein ASY1 are mediated by an interplay between its closure motif and PCH2. Nucleic Acids Res. Published online June 19, 2020. https://doi.org/10.1093/nar/gkaa527.

78. Ye, Q., Lau, R.K., Mathews, I.T., Birkholz, E.A., Watrous, J.D., Azimi, C.S., Pogliano, J., Jain, M., and Corbett, K.D. (2020). HORMA domain proteins and a Trip13-like ATPase regulate bacterial cGAS-like enzymes to mediate bacteriophage immunity. Mol. Cell *77*, 709–722.e7.

79. Voelkel-Meiman, K., Cheng, S.Y., Parziale, M., Morehouse, S.J., Feil, A., Davies, O.R., de Muyt, A., Borde, V., and MacQueen, A.J. (2019). Crossover recombination and synapsis are linked by adjacent regions within the N terminus of the Zip1 synaptonemal complex protein. PLoS Genet. *15*, e1008201.

80. Longtine, M.S., McKenzie, A., 3rd, Demarini, D.J., Shah, N.G., Wach, A., Brachat, A., Philippsen, P., and Pringle, J.R. (1998). Additional modules for versatile and economical PCR-based gene deletion and modification in *Saccharomyces cerevisiae*. Yeast *14*, 953–961.

STAR★METHODS

KEY RESOURCES TABLE

REAGENT or RESOURCE	SOURCE	IDENTIFIER
Antibodies		
Mouse monoclonal α-FLAG M2	Sigma-Aldrich	Cat# F3165;RRID: AB_259529)
Rabbit polyclonal α-Histone H3	Invitrogen	Cat# PA5-31954;RRID: AB_2549427
Rabbit polyclonal α-Histone H3 (phospho Thr11)	Abcam	Cat# ab5168;RRID: AB_304759
Mouse monoclonal α-Cdc5 (4F10)	Médimabs	Cat# MM-0192-1-100
Mouse monoclonal α-GFP (clones 7.1 and 13.1)	Sigma-Aldrich	Cat# 11814460001;RRID: AB_390913
Rabbit α-GFP	This study	N/A
Mouse monoclonal α-Pgk1	Invitrogen	Cat# 459250;RRID: AB_2532235
Rat monoclonal α-alpha Tubulin (YOL1/34)	Santa Cruz Biotechnologies	Cat# sc-53030;RRID: AB_2272440
Rabbit α-Hop1	This study	N/A
Mouse α-Gmc2	Amy MacQueen (Wesleyan University)	[79]
HRP-conjugated Sheep α-Mouse	GE-Amersham	Cat# NA931;RRID: AB_772210
HRP-conjugated donkey α-rabbit	GE-Amersham	Cat# NA934;RRID: AB_772206
FITC-conjugated donkey α-rat	Jackson ImmunoResearch	Cat# 712-095-153;RRID: AB_2340652
DyLight 488 conjugated Donkey α-Mouse	Bethyl Laboratories	Cat# A90-337D2;RRID: AB_10632009
DyLight 594 conjugated Donkey α-rabbit	Bethyl Laboratories	Cat# A120-208D4;RRID: AB_10634260
Chemicals, Peptides, and Recombinant Proteins		
Poly-L-Lysine (0.01%)	Sigma-Aldrich	Cat# P8920
Zymolyase-100T	Amsbio	Cat# 120493-1
RNase A	Sigma-Aldrich	Cat# R4642
Proteinase K PCR grade	Roche	Cat# 03115828001
Complete Mini protease inhibitor mix, EDTA free	Roche	Cat# 11836170001
Salmon sperm DNA	Invitrogen	Cat# AM9680
Protease Inhibitor-Mix HP Plus	SERVA	Cat# 39107
PhoSTOP phosphatase inhibitor mix	Sigma-Aldrich	Cat# 490684501
Proteinase K	VWR	Cat# VWRV0706
HindIII	NEB	Cat# R0104L
Glusulase	Perkin-Elmer	Cat# NEE154001EA
[α-^{32}P]-dCTP	Perkin-Elmer	Cat# BLU513Z250UC
Photo-Flo 200	Kodak	Cat# 146 4510
Vectashield mounting medium with DAPI	Vector Laboratories	Cat# H-1200
β-Estradiol	Sigma-Aldrich	Cat# E8875
Experimental Models: Organisms/Strains		
See supplemental information for yeast strains	This study	N/A
Oligonucleotides		
GV3, 5′ gcc cgt agc cga aat gac tcc 3′, forward *PCH2* check	Sigma-Aldrich	N/A
GV147, 5’ ttg ttt tcg ccg ctg atc 3’, forward out *YCR047c* probe	Sigma-Aldrich	N/A
GV148, 5′ gaa gtt ggg caca at atc, reverse out *YCR047c* probe	Sigma-Aldrich	N/A
GV149, 5′ gga att ccg aga gaa tcg act tgc taa 3′, forward nested *YCR047c* probe	Sigma-Aldrich	N/A
GV150, 5′ gga att cca gcc acc agt ggg ctt ttc 3′ reverse nested *YCR047c* probe	Sigma-Aldrich	N/A
GV999, 5′ gc gcc tcc gtt ggt gga tcc 3′, reverse *PCH2* check	Sigma-Aldrich	N/A

(*Continued on next page*)

Continued

REAGENT or RESOURCE	SOURCE	IDENTIFIER
GV2510, 5′-tca taa aaa tat tct gat ctc aaa ctg aag aca taa aat aag gat gaa ttc gag ctc gtt taa ac −3′, forward *pGAL-3XFLAG-PCH2* tagging	Sigma-Aldrich	N/A
GV2511, 5′ aac cct cag aga tga tcc tcg cac ttg tag gtc aac tat gta gct tcc acc ccc gcc tcc 3′, reverse *pGAL-3XFLAG-PCH2* tagging	Sigma-Aldrich	N/A
Recombinant DNA		
pUC57-*BglII-pGAL-3XFLAG-6xGLY-AscI* (pGV867)	Genewiz Inc.	N/A
pFA6a-*HIS3MX- BglII-pGAL-3XFLAG-6xGLY-AscI* (pGV876)	This study	N/A
Software and Algorithms		
FIJI/ImageJ	National Insititutes of Health (Public Domain)	https://imagej.nih.gov/ij
ImageLab	Bio-Rad	https://www.bio-rad.com
Imaris	Oxford Instruments	https://imaris.oxinst.com
SoftWorX 6.1.1	GE Healthcare Life Sciences	http://incelldownload.gehealthcare.com/bin/download_data/SoftWoRx/7.0.0/SoftWoRx.htm
GraphPad Prism	Graphpad Software, Inc	https://www.graphpad.com/scientific-software/prism/
FloJO	FlowJo LLC	https://www.flowjo.com/solutions/flowjo
Other		
PTFE printed 30-well glass slide	Electron Microscopy Sciences	Cat# 63434-02
BioTrace NT Nitrocellulose	Pall Coorporation	Cat# 66485
Hybond XL	GE Healthcare	Cat# RPN2035
FastPrep-24 5G	MP Biomedicals	Cat# 116005500
DeltaVision Elite	GE Healthcare Life Sciences	https://www.cytivalifesciences.com
Zeiss Axiovert A1	Zeiss	https://www.zeiss.com
Prime-It RmT Random Primer Labeling Kit	Agilent	Cat# 300385
ProbeQuant G-50 Micro column	GE Healthcare Life Sciences	Cat# 8-9034-08
Typhoon TRIO imager	GE Healthcare Life Sciences	N/A

RESOURCE AVAILABILITY

Lead Contact

Further information and requests for resources and reagents should be directed to and will be fulfilled by the Lead Contact, Gerben Vader (gerben.vader@mpi-dortmund.mpg.de)

Materials Availability

All unique/stable reagents generated in this study are available from the Lead Contact without restriction.

Data and Code Availability

This study did not generate/analyze datasets or code.

EXPERIMENTAL MODEL AND SUBJECT DETAILS

Yeast strains and constructs

Budding yeast (*Saccharomyces cerevisiae*) strains used in this study are of SK1 background and their genotypes (and use per Figure panel) are listed in the Supplemental Information (Table S1). For estradiol-dependent induction of *PCH2*, a *pGAL1* promoter fusion with *PCH2* was made as follows: a construct containing *pGAL1* along with a 3xFLAG epitope-6Gly-linker flanked with BglII and AscI (BglII-*pGAL-3xFLAG-6xGLY-AscI*; pGV867) restriction sites were custom synthesized by Genewiz Inc. The construct was cloned in a pFA6a-based precursor plasmid carrying *HIS3MX* (*pFA6a-His3MX6-PGAL1-3XFLAG-6GLY*; pGV876) [80], using standard PCR-based integration, using primers GV2510/GV2511). Correct integration was checked by PCR using primers GV3/GV999.

Growth conditions for synchronous meiosis of budding yeast

Yeast strains were patched onto YP-Glycerol plates and transferred to YP-Dextrose plates (containing 4% glucose). Cells were grown to saturation in liquid YPD culture at room temperature followed by inoculation in pre-sporulation media (BYTA; 50 mM Sodium Phthalate-buffered, 1% yeast extract, 2% tryptone and 1% acetate) at a dilution of A_{600} 0.3. After 18 hours of growth in BYTA at 30°C, cells were washed twice in water and resuspended in sporulation media (0.3% potassium acetate) at A_{600} 1.9 to induce meiosis at 30°C. For *PCH2*-induction experiments, β-estradiol (final concentration 1 μM) was added at indicated time points to induce expression from the *pGAL1* promoter (note that the strains used for this also express a Gal4-ER fusion, as described [73]).

METHOD DETAILS

Flow cytometry

Synchronous cell cycle progression of meiotic cultures was assessed by flow cytometry. 150 μL of sporulation culture was fixed for 2 hours at 4°C in 350 μL 100 % EtOH, and fixed cells were pelleted. Cells were incubated 2 hours at 50°C in 500 μL 50 mM Sodium Citrate with 0.7 μL RNase A (30 mg/ml; Sigma-Aldrich), and subsequently treated with proteinase K (20 mg/ml; VWR) for 2 hours at 50°C. DNA was stained by incubation with 500 μL of 50 mM Sodium Citrate, containing 0.2 μL SYTOX® Green (Life Technologies). Before measurement, cells were disrupted by brief sonication. DNA content of cells was measured using BD Accuri™ C6 (BD Biosciences) flow cytometer, and analyzed using FlowJo Software (FlowJo LLC).

Surface spreading of chromosomes and immunofluorescence

2 mL of meiotic cells were collected at indicated time points, 1% sodium azide was added and processed together after the last time point. Cells were treated with 500 μL of 200 mM Tris pH7.5, 20 mM dithiothreitol (DTT) for 2 min at room temperature followed by spheroplasting at 30 °C in 1 M sorbitol, 2% potassium acetate, 0.13 μg/μL zymolyase for 20 minutes. The spheroplasts were then gently washed two times with 1mL ice-cold MES-Sorbitol solution (1 M sorbitol, 0.1M MES pH 6.4, 1 mM EDTA, 0.5 mM $MgCl_2$) and finally resuspended in 55 μL of the same solution. 20 μL of the resuspended spheroplasts were placed on clean glass slides (dipped in ethanol overnight and air-dried) and two volumes of fixing solution (3% paraformaldehyde, 3.4% sucrose) added to it, followed immediately by adding four volumes of 1% Lipsol. The contents were mixed by gentle rotation of the slide. After one minute, four volumes of the fixing solution were added. A glass rod was used to mechanically spread the chromosomes. The samples were dried overnight at room temperature and stored at −20 °C. For immunofluorescence, slides were treated with 0.4% Photoflo (Kodak) diluted in PBS for 3 minutes. The slides were dipped in PBS with gentle shaking for 5 minutes. Blocking of the samples was done by incubating the samples with 5% BSA in PBS for 15 minutes at room temperature. Overnight incubation with desired primary antibodies (see below) was performed in a humidified chamber at 4°C. The slides were subjected to two washes of 10 minutes each in PBS with gentle shaking followed by incubation with fluorescent-conjugated secondary antibody for 3 hours at room temperature. The slides were again washed twice and mounted using 20 μl of Vectashield mounting media containing 4',6-Diamidine-2′-phenylindole dihydrochloride (DAPI) (Vector Laboratories).

Whole cell immunofluorescence

300 μL of meiotic cells were collected at indicated time points, treated with 1% NaN_3 and processed together after collecting the last time point. Cells were harvested by centrifuging at 3000 rpm for 3 minutes and fixed overnight with 3% paraformaldehyde in 1.2 M Sodium Phosphate buffer. Cells were washed 3 times with phosphate buffer and once with 1.2 M Sodium Sorbitol. Cells were spheroplasted with 1.2 M Sodium Sorbitol, Glusulase (Perkin Elmer), Zymolyase T100 (Amsbio) for 2 hours at 30°C with gentle rotation. Spheroplasted cells were washed once with 1.2 M Sodium Sorbitol and resuspended in 30 μL of the same solution. 5 μL of cells were allowed to settle down on a poly-L-lysine treated well of a PTFE-printed 30-well glass slide for 10 minutes. Samples were treated with ice-cold MeOH for 3 minutes immediately followed by a 10 s treatment with ice-cold acetone. Glass slides were air-dried completely and samples incubated with 4 μL of rat α-Tubulin (diluted 1:100) for 90 minutes. Samples were subsequently washed thrice with PBS followed by a one-hour incubation with 4μL of FITC-labeled secondary antibody (diluted 1:200). Samples were washed 4 times with PBS. Coverslips were mounted using 1 μL Vectashield mounting media per well containing DAPI for staining DNA. Cell cycle progression was checked by counting cells showing separated spindle poles by using tubulin-stained samples. A minimum of 200 cells were counted for each time point using a Zeiss Axiovert A1 (Zeiss) microscope.

Western blotting

Total cell extracts were prepared by harvesting 3 mL of meiotic samples at indicated time points by centrifuging at 3000 rpm for 3 minutes, stored at −20 °C and processed together. Cells were treated with 5% trichloroacetic acid for 10 minutes on ice followed by a wash using ice-cold acetone. Cells were dried overnight and lysed in 200 μL Tris-DTT buffer (Tris pH 7.4, 50 mM EDTA, 5 mM dithiothreitol) using glass beads on a FastPrep-24 5G (MP Biomedicals). 50 μl of 5X-SDS loading buffer was added before resolving the samples by SDS-PAGE, and standard western blotting techniques (using BioTraceNT nitrocellulose; Pall Coorporation), followed by antibody incubation of the samples.

Chromatin fractionation

100 mL of meiotic cells were collected by centrifuging at 3000 rpm for 3 minutes. Cell pellets were washed once in buffer A (150 mM NaCl, 50 mM NaF, 10 mM EDTA, 1 mM NaN_3, respuspended in 1 mL buffer B (100 mM Pipes pH 6.9, 1 mM EGTA, 1 mM $MgCl_2$, 1.2 M Sorbitol) containing 1 mg/ml zymolyase T100 (Amsbio). Cells were spheroplasted for 30 minutes at 37°C, and collected by centrifuging at 2000 rpm for 5 minutes at 4°C. Spheroplasts were washed in 1.2 M Sorbitol, and resuspended in 250 μL buffer C (25 mM MOPS pH 7.2, 15 mM MgCl2, 15 mM EGTA, 1.2 M Sorbitol, 0.5% Triton X-100, 1 mM dithiothreitol, 60 mM β-glycerophosphate, 0.2 mM Na_3VO_4, 1 mM phenylmethylsulfonylfluoride, 1 Complete Mini EDTA-free (Roche) pil/10 ml, Protease Inhibitor-Mix HP Plus (Serva), and 1 PhoSTOP (Sigma-Aldrich) pil/10 ml)), and incubated at 4°C for 5 minutes. Total lysate (50 μl) was collected, and remaining suspension was centrifuged at 14000 rpm for 20 minutes 4°C. The supernatant (= soluble fraction) was collected, and pellet was washed twice in 300 μL buffer C. Pellet was resuspended in 200 μL buffer C and collected (= chromatin fraction). Fractions were precipitated by addition of 10% trichloroacetic acid, and incubated for 30 minutes at 4°C. Pellets were centrifuged (14000 rpm for 1 minute 4°C) and washed with 100% Acetone. Precipitated fractions were resuspended in 7 M Urea, 2% SDS, 50 mM TRIS pH 7.5, and analyzed by western blotting.

Genomic DNA isolation, digestion and Southern blotting

10 mL of meiotic samples at indicated time points by centrifuging at 3000 rpm for 3 minutes, stored at −20 °C and processed together. Cells were spheroplasted for 45 minutes at 37°C in spheroplasting buffer (1 M Sorbitol, 42 mM K_2HPO_4, 8 mM KH2PO_4, 5 mM EDTA) supplemented with β-mercaptoethanol and 250 μg/ml zymolyase T100. Spheroplasts were lysed by addition of 100 μL of lysing buffer (0.5 M Tris pH 8, 0.25 M EDTA, 3%SDS) and 15 μL PCR-grade Proteinase K (Roche) and incubated at 65°C for 120 minutes. 150 μL 5M KoAc was added, and lysates were incubated at 4°C for 20 minutes. Lysates were centrifuged (14000 rpm, for 20 minutes at 4°C), and supernatant was added to 750 μL EtOH. Precipitate was spun down (14000 rpm, for 20 minutes at 4°C), and dissolved in 750 μL TE (10 mM Tris, pH 8, 1 mM EDTA) supplemented with 50 μg/ml RNase A (Sigma), by incubation at 37°C for 30 minutes, followed by incubation at 4°C for 14 hours. 500 μL phenol/chloroform/isopropanol (25:24:1; Carl Roth) was added, which was gently mixed by inverting 60 times. The solution was centrifuged for phase separation for (14000 rpm, for 10 minutes at 4°C). 600 μL of the DNA-containing upper phase was added to 750 μL isopropanol. DNA was recovered by centrifugation (14000 rpm, for 10 minutes at 4°C), washed with 70% EtOH, and centrifuged (14000 rpm, for 10 minutes at 5°C). DNA was dissolved in 125 μL TE. Genomic DNA was digested HindIII (NEB) for 4 hours at 37°C. 35 μL of genomic DNA was added to 30 μL of 10x NEB buffer, 2.5 μL HindIII and 232.5 μL dH_20. Digested DNA was precipitated by addition of 25 μL 3 M NaOAc (pH 5.5) and 650 μL EtOH at −20°C for 30 minutes. DNA was centrifuged (14000 rpm, for 10 minutes at 4°C). Pellet was resuspended in 15 μL TE. 5 μL loading buffer (1 mL loading buffer contains 400 μL 10x NEB3 buffer and 600 μL 10x loading buffer) was added. DNA was separated on a 0.6% SeaKem® LE agarose (Lonza) gel for 16 hours at 70 V in an Owl™ A2-BP large gel system (Thermo Fisher Scientific) containing TBE buffer. Separated DNA bands were visualized by UV light after staining the gel in a EtBr bath for 30 min at room temperature. The agarose gel was incubated with 0.25 M HCl for 40 minutes with gentle shaking. DNA was denatured with 0.4 M NaOH for 35 minutes. Whatman filter paper (20 × 35 cm) was placed on an inverted gel tray in the Owl™ A2-BP large gel system (Thermo Fisher Scientific). The wick was wetted with 0.4 M NaOH. Two gel-size pieces of Whatman paper were placed on the wick and soaked with NaOH, and the gel was placed on top, and a pre-soaked (dH_20) Hybond XL membrane (GE Healthcare) was added. Two wetted Whatman papers were placed on the membrane, and surrounded by Parafilm, and 20 paper towels were placed on top. Sufficient transfer of the DNA from the gel to the membrane was achieved overnight. The membrane was rinsed 30 min in 50 mM sodium phosphate buffer, pH 7.2. Membranes were pre-hybridized in pre-warmed glass bottles filled with 20 mL of hybridization solution (0.25 mM Sodium Phosphate pH 7.2, 0.25 M NaCl, 1 mM EDTA, 7% SDS, 5% Dextran Sulfate) and 300 μL of denatured salmon sperm DNA for at least 30 minutes (65°C) in an HB-1000 hybridization oven (Analytik). DNA probe *YCR047C* (SGD, chromosome *III* ; 209,361-210,030, amplified from genomic DNA by nested PCR with primers GV147/GV148, and GV149/GV150) was labeled with [α-^{32}P]-dCTP (Perkin Elmer) with the Prime-It RmT Random Primer Labeling Kit (Agilent Technologies). Labeled probes were purified using an illustra ProbeQuant G-50 Micro column (GE Healthcare), denatured for 10 min at 95°C and cooled to 4°C. Denatured probe was added to the membrane and hybridized at 65°C for 14 hours. Membranes were washed with 120 mL of low stringency SSC buffer (0.3 M NaCl, 30 mM Sodium citrate, 0.1% SDS) for 15 minutes and with 120 mL of high stringency SSC buffer ((15 mM NaCl, 1,5 mM Sodium citrate, 0.1% SDS)) for 30 minutes at 65°C. Hybridization signals were quantitated using a Typhoon TRIO imager (GE Healthcare). DNA double-strand break intensities were determined using Fiji/ImageJ (NIH).

Antibodies

Chromosome surface spreads were immunostained with mouse α-GFP (Sigma-Aldrich, diluted 1:50), mouse α-Gmc2 (a kind gift from Amy MacQueen, Wesleyan University, Middletown, CT, USA, diluted 1:200 [79]), goat α-Zip1 (Santa Cruz Biotechnology, diluted 1:100) and rabbit α-Hop1 (made in-house, diluted 1:200). α-Hop1 production was performed at the antibody facility of the Max-Planck-Institute of Molecular Cell Biology and Genetics (Dresden, Germany) using affinity purified full length 6-His-tagged Hop1. For whole cell immunofluorescence, rat α-Tubulin (Abcam, diluted 1:100) was used. DAPI was used to stain the DNA in both cases. Following antibodies with respective dilutions were used for western blot of the protein extracts: rabbit α-Hop1 (made in-house; 1:10000), mouse α-Pgk1 (Thermo Fischer, 1:5000); rabbit α-phospho-Histone-H3-Thr11 (Abcam, 1:1000), mouse α-Flag (Sigma-Aldrich,1:1000), mouse α-Cdc5 (Medimabs, 1:1000), rabbit α-GFP (made in-house, 1:5000).

QUANTIFICATION AND STATISTICAL ANALYSIS

Microscopy and cytological analysis

Images were acquired at room temperature using 100X1.42 NA PlanApo-N objective (Olympus) on a DeltaVision imaging system (GE Healthcare) equipped with an sCMOS camera (PCO Edge 5.5). Serial z-stacks of 0.2 μm thickness were obtained and deconvolved using SoftWoRx software 6.1.l. (GE Healthcare). Image quantifications for Zip1, Hop1 and Gmc2 intensity on the chromosomes were done using Imaris 7.6.4 32-bit software (Bitplane). The 'Surface' function was applied to the raw images on DAPI channel to identify the DNA. Values for the sum total fluorescence intensity and volume were obtained. The background was calculated using the 'Spots' function by manually placing three ROIs in a region that lacked DNA. Average background intensity adjusted for volume was subtracted from the chromosomal intensities of different proteins to obtain a sum of total fluorescence intensity corrected for the background. For representative images, maximum intensity projection images were obtained and processed using ImageJ software. Scatterplots were generated using Graphpad Prism.

Statistical analysis

Statistical analyses were performed using Graphpad Prism or Ecxel. Statistical analyses for microscopy were done using an unpaired, nonparametric Mann-Whitney U-test with computation of two-tailed exact p values. Significance was determined using p values (> 0.05 (ns); ≤ 0.05 (*); ≤ 0.01 (**); ≤ 0.001 (***); ≤ 0.0001 (****)). Details of statistical analyses for each experiment can be found in Supplemental Information, and information is indicated in the corresponding figure legends.